

Human Pose Transfer with Disentangled Feature Consistency

Kun Wu, Chengxiang Yin, *Student Member, IEEE*, Zhengping Che, *Member, IEEE*, Bo Jiang, Jian Tang, *Fellow, IEEE*, Zheng Guan, *Member, IEEE*, and Gangyi Ding, *Senior Member, IEEE*

Abstract—Deep generative models have made great progress in synthesizing images with arbitrary human poses and transferring poses of one person to others. However, most existing approaches explicitly leverage the pose information extracted from the source images as a conditional input for the generative networks. Meanwhile, they usually focus on the visual fidelity of the synthesized images but neglect the inherent consistency, which further confines their performance of pose transfer. To alleviate the current limitations and improve the quality of the synthesized images, we propose a pose transfer network with Disentangled Feature Consistency (DFC-Net) to facilitate human pose transfer. Given a pair of images containing the source and target person, DFC-Net extracts pose and static information from the source and target respectively, then synthesizes an image of the target person with the desired pose from the source. Moreover, DFC-Net leverages disentangled feature consistency losses in the adversarial training to strengthen the transfer coherence and integrates the keypoint amplifier to enhance the pose feature extraction. Additionally, an unpaired support dataset MIXAMO-SUP providing more extra pose information has been further utilized during the training to improve the generality and robustness of DFC-Net. Extensive experimental results on MIXAMO-POSE and EDN-10K have demonstrated DFC-Net achieves state-of-the-art performance on pose transfer.

Index Terms—Human pose transfer, Generative adversarial network, Image generation, Computer vision

I. INTRODUCTION

HUMAN pose transfer has become increasingly compelling recently since it is closely related to movies' special effects [1], reenactment [2], entertainment systems [3] and so forth [4]. Given some images of a target person and a source person image with the desired pose (e.g., judo, dance), the goal of the human pose transfer task is to synthesize a realistic image of the target person with the desired pose of the source person.

With the power of deep learning, especially the generative adversarial networks (GANs) [5], [6], [7], pioneering works have raised impressive solutions to address the human pose transfer by efficiently leveraging the image-to-image translation schemes and have achieved significant progress. Intu-

itively, early routine coarsely conducts human pose transfer through general image-to-image translation methods such as Pix2Pix [8] and CycleGAN [9], which attempt to translate the extracted skeleton image of source person to the image of target person with the desired poses. Subsequent approaches adopt specifically designed modules for human pose transfer, which are also built upon image-to-image translation methods and utilize the skeleton images as the start point.

However, most existing works utilize the pose estimator [10], [11], [12] as preprocessing operations to generate the pose images from the source images and try to memorize the pose-to-image mappings only through generators in the adversarial training to ensure the visual fidelity of the synthesized images, which makes them difficult to transfer complex poses on the same person and further impedes pose transfer between people with different static (background and person appearance) and pose information simultaneously. We observe that the commonly used reconstruction loss and the adversarial generative loss only constrain the synthesized image generation in image-level and pixel-level, respectively. And these approaches lack the consistencies of pose and static since they do not explicitly extract pose and static information in a decoupled way between the synthesized and real images.

Towards alleviating the mentioned limitations, it is necessary to exploit the disentangled pose and static feature consistencies between the synthesized and real images, i.e., the synthesized target image should have a similar high-level static feature to the real target person as well as a similar high-level pose feature to the real source person. The disentangled pose and static feature consistencies can constrain the training in feature-level and lead to a more consistent and realistic synthesized result. Thus, it is crucial to disentangle the pose and static information while ensuring consistency between the input images and the synthesized images when designing the model, and enhance its generality by incorporating extra unpaired dataset during the training. Moreover, an accurate benchmark for evaluating human pose transfer between different people is required since existing datasets cannot support such a task.

In this paper, we propose a pose transfer network with Disentangled Feature Consistency (DFC-Net) to facilitate human pose transfer. DFC-Net contains a pose feature encoder and a static feature encoder to extract pose and static features from the source and target person, respectively. Notably, a pre-trained pose estimator such as OpenPose [13] has been integrated into the pose feature encoder to extract the keypoint heatmaps. In order to remedy the distortion of the extracted

Kun Wu and Chengxiang Yin are with Department of Electrical Engineering and Computer Science, Syracuse University, Syracuse, NY, 13244. E-mail: {kwu102, cyin02}@syr.edu

Zhengping Che and Bo Jiang are with Didi Chuxing, China. E-mail: {chezhengping, scottjiangbo}@didiglobal.com

Jian Tang is with Midea Group, China. E-mail: tangjian22@midea.com

Zheng Guan and Gangyi Ding are with the Computer Science School, Beijing Institute of Technology, China. E-mail: {guanzheng_bit, ding-gangyi_bit}@hotmail.com

Corresponding author: Jian Tang

keypoints caused by pose estimator, we introduce a keypoint amplifier to eliminate the noise in keypoint heatmaps by enlarging the gap between large and small values in it. An image generator synthesizes a realistic image of the target person conditioned on the disentangled pose and static features. The feature encoders and image generator empower DFC-Net to enable us to present novel feature-level pose and static consistency losses [9]. These losses reinforce the consistency of pose and static information in the feature space and simultaneously maintain visual fidelity. Additionally, to further improve the robustness and generality of DFC-Net, by disentangling the pose information from the source person, we present a general scheme, which builds an extra unpaired support set called MIXAMO-SUP, providing different people with unseen poses in the training set as the source images with consistency losses.

Inspired by [14], we collect an animation character image dataset named MIXAMO-POSE from Adobe Mixamo [15], a 3D animation library, to accurately generate different characters performing the identical poses as a benchmark to assess the human pose transfer between different people. MIXAMO-POSE contains four different animation characters performing 15 kinds of poses. To further evaluate the DFC-Net, we also modify a real person dataset called EDN-10K upon [16], which contains 10K images for four real subjects performing different poses. The experimental results on these two datasets demonstrate that our model can effectively synthesize realistic images and conduct pose transfer for both the animation characters and real persons.

In summary, our contributions are as follows:

- We propose a novel method DFC-Net for human pose transfer with two disentangled feature consistency losses to make the information between the real images and synthesized images consistent.
- We introduce a keypoint amplifier to denoise the keypoint heatmaps and utilize an extra unpaired dataset to further improve the generality of our model.
- We collect an animation character dataset MIXAMO-POSE as a new benchmark to enable the accurate evaluation of pose transfer between different people.
- We conduct extensive experiments on datasets MIXAMO-POSE and EDN-10K, on which the empirical results demonstrate the effectiveness of our method.

II. RELATED WORK

Generative adversarial networks (GANs) [5] have achieved tremendous success in image-to-image translation tasks, whose goal is to convert images from one domain to a different domain. Pix2Pix [8] proposes a framework based on cGANs [17] with an encoder-decoder architecture [18]; CycleGAN [9] addresses this problem by using a cycle-consistent GANs; DualGAN [19] and [20] are also unsupervised image-to-image translation methods trained on unpaired dataset. Similarly, [21], [22], [23] are also image-to-image translation techniques, but they try to generate a dataset of the target domain with labels for domain adaptation tasks. The above works can be exploited as a general approach in the human pose transfer

task, while the precondition is that they have a specific image domain which can be converted to the synthesized image domain, e.g., using a pose estimator [12] to generate a paired skeleton image dataset. Different from the image-to-image translation methods, DFC-Net does not need to generate an extra skeleton image dataset and form a paired dataset.

Specifically, there is a growing number of human pose transfer methods [24], [25], [26] proposed to synthesize a person image given the desired pose. PG² [27] presents a two-stage method using U-Net to synthesize the target person with arbitrary poses. [28] further decomposes an image into the foreground, background and pose features to achieve more precise control of different information. [29] introduces a warping method for image and corresponding pose by spatial transformer networks (STN) [30]. [31] introduces a multi-stage GAN loss and synthesizes each body part, respectively. [32] leverages the DensePose [33] rather than the commonly used 2D key-points to perform accurate pose transfer. [16] learns a direct mapping from the skeleton images to synthesized images with corresponding pose based on the architecture of Pix2PixHD [34].

Besides, other methods focus on the spatial transformation capability of the models. [35] builds deformable skip connections to move information and transfer textures. Monkey-Net [36] encodes pose information via dense flow fields generated from keypoints learned in a self-supervised fashion. First-Order Motion Model [37] decouples appearance and pose and proposes to use learned keypoints and local affine transformations to generate image animation. However, it is difficult for both the Monkey-Net and First-Order Motion Model to extract the keypoints information of a person who is not in the training dataset, which drops performance when transferring pose from a new person. [38] integrates the human pose transfer, appearance transfer and novel view synthesis into one unified framework by using SMPL [39] to generate human body mesh.

Most of the existing methods start from a preprocessed skeleton or pose image dataset and only memorize the pose-to-image mappings only through generators in the adversarial training, which can not generalize well on complex poses. In contrast, our method directly takes the original images as input and learns to disentangle and reassemble the pose and static features. By disentangling the pose and static features, we can enforce the feature consistencies between the synthesized and real images, and leverage the pose features from an unpaired dataset to improve performance.

III. METHODOLOGY

A. Overview

Given one image x_s of a source person and another image x_t of a target person, DFC-Net synthesizes an image x_{syn} , which reserves a) the pose information, e.g., pose and location, of the source person in x_s , and b) the static information, e.g., person appearance and environment background, from the target image x_t . For each image, DFC-Net attempts to disentangle the pose and static information into orthogonal features. Specifically, DFC-Net consists of the following core

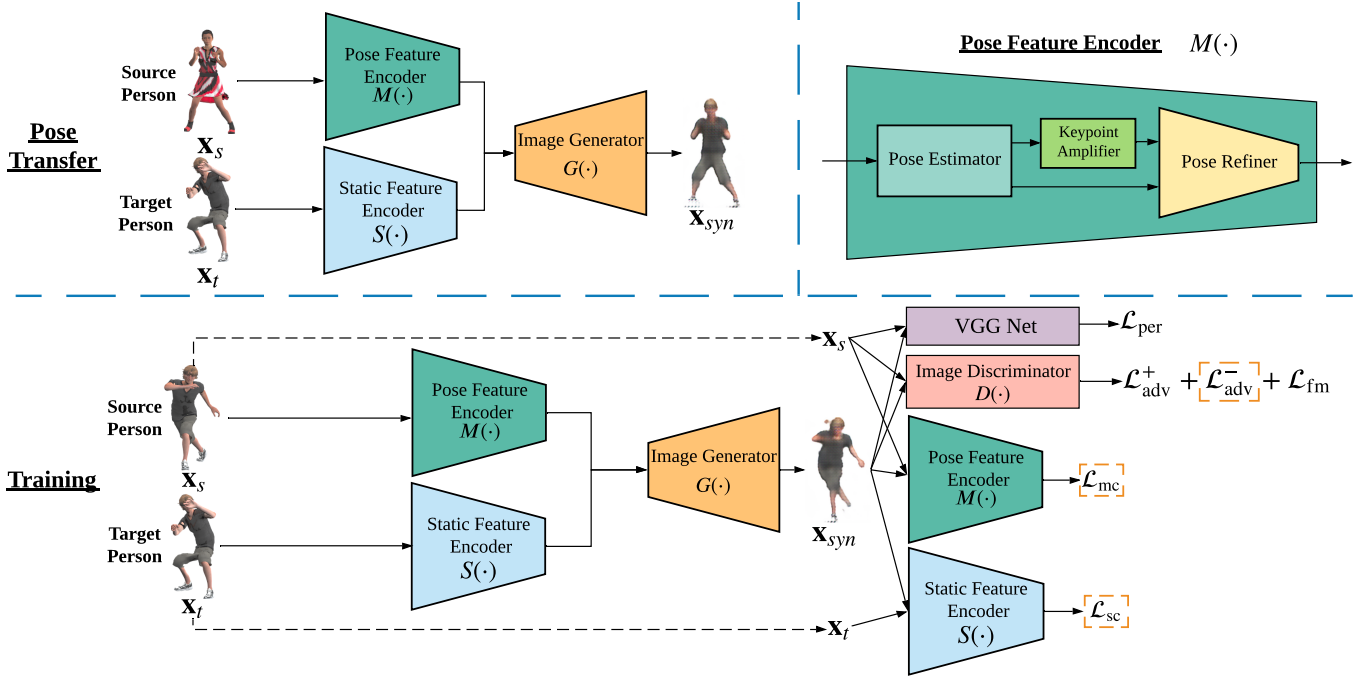


Fig. 1: **Upper left:** DFC-Net synthesizes an image of the target person performing the pose of the source person. **Upper right:** the Pose Feature Encoder $M(\cdot)$ includes three components: pre-trained Pose Estimator, Keypoint Amplifier and Pose Refiner. **Bottom:** the overview of training process of DFC-Net. Note that for training with support set only the losses \mathcal{L}_{adv}^- , \mathcal{L}_{mc} and \mathcal{L}_{sc} surrounded by orange dotted boxes are summed as \mathcal{L}_{sup} .

components: 1) a *Pose Feature Encoder* $M(\cdot)$, which extracts pose features $M(x)$ from an image x ; 2) a *Static Feature Encoder* $S(\cdot)$, which extracts static features $S(x')$ from an image x' ; and 3) an *Image Generator* $G(\cdot)$, which synthesizes an image $G(M(x), S(x'))$ based on the encoded pose and static features $M(x)$ and $S(x')$ from images x and x' separately.

In the remainder of this section, we describe the model architecture and introduce the training procedure, followed by the model instantiations.

B. Pose Transfer Network Architecture

The architecture of the proposed model is shown in Figure 1.

1) *Pose Feature Encoder*: Our designed Pose Feature Encoder consists of a Pose Estimator network, a Keypoint Amplifier block, and a Pose Refiner network. Even if the pre-trained pose estimator (OpenPose [13] in our implementation) is good enough, since it is pre-trained on COCO keypoint challenge dataset [40], when applied on MIXAMO-POSE and EDN-10K datasets with different distributions, more noise are made on keypoint heatmaps.

Given a RGB image $x \in \mathbb{R}^{3 \times H \times W}$ of height H and width W , the pre-trained *Pose Estimator* aims at extracting pose information $P(x)$ from the image x . Similar to [12], the extracted pose information contains the downsampled keypoint heatmaps $h \in \mathbb{R}^{18 \times \frac{H}{8} \times \frac{W}{8}}$ and the part affinity fields $p \in \mathbb{R}^{38 \times \frac{H}{8} \times \frac{W}{8}}$. The keypoint heatmaps h store the heatmaps of 18 body parts, and the part affinity fields p store the location and orientation for heatmaps of body parts and background, which has 38 ($= (18 + 1) \times 2$) channels.

As there might be much noise in the estimated keypoint heatmaps h , we apply a softmax function with a relatively small temperature T (e.g., 0.01) as the *Keypoint Amplifier* to denoise the extracted keypoint heatmaps by increasing the gap between large and small values in the heatmaps and obtain the amplified heatmaps h' by

$$h' = \text{softmax} \left(\frac{1}{T} \cdot h \right). \quad (1)$$

By employing Keypoint Amplifier on the input heatmaps, the small probability, e.g., 0.2, will be squeezed to almost 0.0. On the contrary, the large probability, e.g., 0.8, will be squeezed to almost 1.0. Without the Keypoint Amplifier, the generator may still synthesize blurry limbs for the low probability areas and twist the generated person.

Finally, the *Pose Refiner* takes both the part affinity fields p and the amplified keypoint heatmaps h' and produces the encoded pose feature vector $M(x)$. In this way, the pose information extracted from the Pose Estimator can be refined, and the influence caused by different limb ratios and/or camera angles and distances can be reduced.

2) *Static Feature Encoder*: While the Pose Feature Encoder is not capable of extracting static information, the static information including background, person appearance, etc., from another image x' are captured automatically by another network. Named as Static Feature Encoder, this module extracts only static features $S(x')$ from x' .

3) *Image Generator*: Given pose features $M(x_s)$ extracted from a source image x_s and static features $S(x_t)$ extracted

from a target image \mathbf{x}_t , the Image Generator outputs the synthesized image \mathbf{x}_{syn} by

$$\mathbf{x}_{\text{syn}} = G(M(\mathbf{x}_s), S(\mathbf{x}_t)). \quad (2)$$

It is noting that many existing methods (e.g., [16]) attempt to learn pose-to-image or pose-to-appearance mapping solely via its generator, which poses a difficult task on parameterizing the static information of the target in the generator. Meanwhile, with the same generator, the desired pose information of \mathbf{x}_s may fail to synthesize if the unseen pose is very different from the poses in the training set. DFC-Net, instead, extracts and utilizes decomposed static and pose features, which enables the reconstruction’s quality improvement.

C. Training DFC-Net

We train the pose transfer network in an adversarial learning way with disentangled feature consistency losses as well as other objectives. Basically, the model is trained with a set of images of the same person, possibly from one or several video clips. To further improve the generalization ability of DFC-Net, we propose to train DFC-Net with a support set and give more details later. We show the ablation study results in Section IV-C.

1) *Adversarial Training*: We employ an *Image Discriminator* (D) in an adversarial learning way to ensure the synthesized image \mathbf{x}_{syn} borrows the pose and static information from the source and target images (\mathbf{x}_s and \mathbf{x}_t) separately. As both the source and target images during training contain the same person with the same appearance and background, they share almost the same static features, i.e., $S(\mathbf{x}_t) \simeq S(\mathbf{x}_s)$. Therefore, the output of the model \mathbf{x}_{syn} can also be treated as a reconstruction of the source image \mathbf{x}_s , as the synthesized images contain the same pose features $M(\mathbf{x}_s)$ as the source image. This inspires us to resort to the conditional generative adversarial network (cGAN) [8], where the Image Discriminator attempts to discern between the real sample \mathbf{x}_s and the generated image \mathbf{x}_{syn} , conditioned on the pose features $M(\mathbf{x}_s)$ extracted from the source image. That is, the Image Discriminator attempts to fit $D(\mathbf{x}_s, M(\mathbf{x}_s)) = 1$ and $D(\mathbf{x}_{\text{syn}}, M(\mathbf{x}_s)) = 0$. The adversarial loss is described as follows:

$$\mathcal{L}_{\text{adv}} = -(\mathcal{L}_{\text{adv}}^+ + \mathcal{L}_{\text{adv}}^-), \quad (3)$$

where

$$\mathcal{L}_{\text{adv}}^+ = \log D(\mathbf{x}_s, M(\mathbf{x}_s)), \quad (4)$$

$$\mathcal{L}_{\text{adv}}^- = \log(1 - D(\mathbf{x}_{\text{syn}}, M(\mathbf{x}_s))). \quad (5)$$

We enhance the Image Discriminator with a multi-scale discriminator $D = (D_1, D_2)$ [34] and include the discriminator feature matching loss \mathcal{L}_{fm} in our objective. The feature matching loss is a weighted sum of feature losses from 5 different layers of the Image Discriminator, calculated by L_1 distance between the corresponding features of \mathbf{x}_s and \mathbf{x}_{syn} .

In order to increase the training stability and improve the synthesized image quality, we also add the perceptual loss \mathcal{L}_{per} [41] based on a pre-trained VGG network [42].

2) *Disentangled Feature Consistency Losses*: The above adversarial training losses aim at penalizing discrepancy between the synthesized and source images directly in the raw image space. To improve the accuracy and robustness of the pose transfer results, we also introduce two disentangled feature consistency losses in terms of *pose* and *static* features to assure the synthesized person looks like the target person and behaves as the source person separately. The pose consistency loss \mathcal{L}_{mc} measures the differences between the synthesized and source images in the pose feature space, and the static consistency loss \mathcal{L}_{sc} measures the differences between the synthesized and target images in the static feature space. They are both L_1 distances between the outputs from the corresponding encoders, formally defined as

$$\mathcal{L}_{\text{mc}} = \|M(\mathbf{x}_{\text{syn}}) - M(\mathbf{x}_s)\|_1, \quad (6)$$

$$\mathcal{L}_{\text{sc}} = \|S(\mathbf{x}_{\text{syn}}) - S(\mathbf{x}_t)\|_1. \quad (7)$$

3) *Full Objective*: By bringing all the objective terms together, we train all components jointly except for the Pose Estimator to minimize the full objective $\mathcal{L}_{\text{full}}$ below.

$$\mathcal{L}_{\text{full}} = \lambda_{\text{adv}}\mathcal{L}_{\text{adv}} + \lambda_{\text{fm}}\mathcal{L}_{\text{fm}} + \lambda_{\text{per}}\mathcal{L}_{\text{per}} + \lambda_{\text{mc}}\mathcal{L}_{\text{mc}} + \lambda_{\text{sc}}\mathcal{L}_{\text{sc}} \quad (8)$$

where $\lambda_{\text{adv}}, \lambda_{\text{fm}}, \lambda_{\text{per}}$ are set to 1, 10, 10 following Pix2Pix [8] and Everybody Dance Now (EDN) [16], while $\lambda_{\text{mc}}, \lambda_{\text{sc}}$ are set to 0.1, 0.01 by grid search. We set the λ_{sc} to 0.01 comparing to the λ_{mc} to balance the \mathcal{L}_{mc} and \mathcal{L}_{sc} .

4) *Training with Support Set*: Through disentangling the pose feature from the source images, source images \mathbf{x}_s with different persons can be adopted as input in the training process to improve the generalization ability of our model. These images, referred to as the *support set*, provide many kinds of unseen poses. Note that the subjects in *support set* can be arbitrary and are different from the primary training dataset. Therefore, the two input images share different static features, i.e., $S(\mathbf{x}_t) \neq S(\mathbf{x}_s)$, and the ground-truth image with the target person performing the pose of the source person is not available at all. As a result, the corresponding losses $\mathcal{L}_{\text{adv}}^+, \mathcal{L}_{\text{per}}$ and \mathcal{L}_{fm} for the support set are not applicable, and we only optimize relevant objective terms, which is defined by

$$\mathcal{L}_{\text{sup}} = \lambda_{\text{adv}}\mathcal{L}_{\text{adv}}^- + \lambda_{\text{mc}}\mathcal{L}_{\text{mc}} + \lambda_{\text{sc}}\mathcal{L}_{\text{sc}} \quad (9)$$

where the weights $\lambda_{\text{adv}}, \lambda_{\text{mc}}, \lambda_{\text{sc}}$ remain the same as for the full objective in Equation 8.

D. Implementation details

We employed the pre-trained VGG-19 [43] network part from [12] for the Pose Estimator, and adopted the similar approach in [44] to build our network, the detailed designs are as follows:

- **Pose Refiner**: It is composed of a convolutional block, a channel-wise upsampling module and five residual blocks [45]. Firstly, the convolutional block consists of a reflection padding layer, a 7×7 convolutional layer, a

batch normalization layer and ReLU. The channel-wise upsampling module, which increases the number of the channel from 64 to 512, contains three convolutional blocks. Each block contains a 3×3 convolutional layer, a batch normalization layer and ReLU. Each of the five residual blocks consists of two small convolutional blocks and each block has a reflection padding layer, a 3×3 convolutional layer, a batch normalization layer. The first small convolutional block also has a ReLU at the end.

- **Static Feature Encoder:** It firstly has the same convolutional block as in the Pose Refiner. Then it contains three convolutional downsampling blocks and each block consists of a 3×3 convolutional layer, a batch normalization layer and ReLU. There are also five residual blocks following the downsampling blocks as the same as in the Pose Refiner.
- **Image Generator:** It is composed of four residual blocks, an upsampling module and a convolutional block. Each of the residual blocks is the same as in the Pose Refiner and Static Feature Encoder. The upsampling module consists of three transposed convolutional blocks and each block is composed of a 3×3 transposed convolutional layer, a batch normalization layer and ReLU. The last convolutional block contains two reflection padding layers, two 7×7 convolutional layers and a tangent function.
- **Image Discriminator:** It contains two discriminators at different scales, which are similar to [34]. For each discriminator it is composed of five convolutional blocks. The first block has a 4×4 convolutional layer and LeakyReLU. Each of the next three blocks has a 4×4 convolutional layer, a batch normalization layer and LeakyReLU. The last block only has a 4×4 convolutional layer.

IV. EXPERIMENTS

A. Experimental Setup

1) *Datasets:* We built MIXAMO-SUP as support set, to boost the generality of DFC-Net and organized two datasets, MIXAMO-POSE and EDN-10K, to verify the effectiveness of the proposed DFC-Net for human pose transfer.

- **MIXAMO-POSE:** We randomly chose 4 characters, *Andromeda*, *Liam*, *Remy* and *Stefani*, with 30 different pose sequences from Mixamo. To render the 3D animations into 2D images, we loaded each character performing each pose sequence on a white background into Blender [46], placed two cameras in front of and behind the character, and took the images. We centered the characters in the images according to their keypoints and resized them to 256×256 . MIXAMO-POSE were split into training and test sets. For each character, the training set contains 1488 images with 15 poses, and the test set contains 1185 images with 15 other poses.
- **EDN-10K:** We processed and tailored the dataset released by [16] to build the EDN-10K dataset. The original dataset consists of five long target videos, each lasting from 8 minutes to 17 minutes and split into the training and test set. We chose the first four subjects since the subject five only performed less complex dance poses.

In each video of the original dataset, a different subject performed a series of different motions, and the camera was fixed to keep the background unchanged. We chose four subjects from the original dataset, uniformly sampled 10k frames as the training set and 1k frames as the test set for each subject. Since the original images have a large resolution of 1024×512 and most areas are the fixed background, we cropped all frames to the middle 512×512 square areas and resized them to 256×256 .

- **MIXAMO-SUP:** We built a *support set* by rendering 15684 images of six new characters from Mixamo [15] with another 15 unseen poses in the same way as MIXAMO-POSE. DFC-Net leveraged the support set as the source person images, it is unnecessary to contain the same person as the target person image. When training on both EDN-10K and MIXAMO-POSE, we use MIXAMO-SUP as the support set. Note that MIXAMO-SUP has a totally different distribution from EDN-10K but still gains a huge improvement shown in Section IV-C.

For each character or subject in MIXAMO-POSE and EDN-10K, we train one separate model following the same scheme of [16]. The experiments on MIXAMO-POSE include the pose transfer both on the different people, e.g., transfer the unseen pose of *Liam* to *Andromeda*, and the same person, e.g., transfer the unseen pose of *Andromeda* to herself. The experiments on EDN-10K only include the pose transfer on the same person because the ground-truth of different people carrying the same pose are unavailable.

2) *Baseline Methods:* We compared our DFC-Net with the following competitive baselines:

- **Nearest Neighbors (NN):** For each source person image \mathbf{x}_s , we chose the image \mathbf{x}' in the training set \mathcal{D}_{tr} with the lowest mean square error (MSE) between the pose information $P(\mathbf{x}_s)$ and $P(\mathbf{x}')$ as \mathbf{x}_{syn} .

$$\mathbf{x}_{syn} = \arg \min_{\mathbf{x}' \in \mathcal{D}_{tr}} \|P(\mathbf{x}_s) - P(\mathbf{x}')\|_2^2. \quad (10)$$

The pose information was extracted by the same Pose Estimator as in our method.

- **Pose-guided Methods:** We chose CycleGAN [9], Pix2Pix [8] and Everybody Dance Now (EDN) [16] as the baselines. They all took the skeleton images as input instead of the original images, we employed a pre-trained pose estimator [12] to extract keypoints, used OpenCV [47] to connect pairs of keypoints with different colors to generate the skeleton images. To ensure fair comparisons, the face GAN and face keypoint estimator in EDN were not adopted in our implementation, as they are independent components and can be seamlessly adopted by other learning-based baselines.
- **Spatial Transformation Methods:** We selected Liquid Warping GAN (LWG) [38], Monkey-Net (MKN) [36] and First Order Motion Model (FOMM) [37]. LWG calculates the flow fields with additional 3D human models and integrates the human pose transfer, appearance transfer and novel view synthesis into one unified framework. MKN and FOMM are both object-agnostic frameworks using learned keypoints to generate image animation in a self-supervised fashion.

3) *Evaluation Metrics*: We evaluated the quality of the synthesized images with three commonly used metrics:

- **MSE**: The mean squared error between the values of pixels of synthesized images and ground-truth images. *Lower* MSE values are better.
- **PSNR**: The peak signal-to-noise ratio, which provides an empirical measure of the quality of synthesized images regarding ground-truth images. *Higher* PSNR values are better.
- **SSIM**: Structural similarity [48], which is another perceptual metric that quantifies the quality of synthesized images given ground-truth images and focuses more on structural information (e.g., light). *Higher* SSIM values are better.

We calculated the average scores among all pairs of synthesized and ground-truth images on the test set. On MIXAMO-POSE, for each character as the target person, we reported the average metrics of 4 different characters as the source person. While on EDN-10K, we reported metrics of the task on the same person for every subject.

B. Quantitative Evaluations

1) *Results on MIXAMO-POSE*: Tables I, II and III respectively show the quantitative results of pose transfer in terms of MSE, SSIM and PSNR on the MIXAMO-POSE dataset. Summarizing the aboving tables, Table IV shows the average quantitative results of pose transfer in terms of three metrics on MIXAMO-POSE. We obtained the empirical results clearly demonstrated the effectiveness of DFC-Net on animation images:

- Our DFC-Net outperformed all competing baselines regarding all three metrics on average. Notably in terms of MSE, DFC-Net outperformed the second best by 0.82.
- MKN and FOMM dropped their performance when they transferred the pose between different people. It is difficult for them to extract keypoints features without a pre-trained pose estimator when the source person was not in the training dataset.

2) *Results on EDN-10K*: Tables V, VI and VII depict results in terms of MSE, SSIM and PSNR on the EDN-10K dataset. Table VIII depicts the average results of 4 subjects on the EDN-10K dataset. The experimental results validated the advances of DFC-Net for real images:

- Our method consistently outperformed all the baseline methods on all subjects. For instance, our method achieved the highest average SSIM of 0.8269 for all subjects, while no other methods except MKN got SSIM score greater than 0.8.
- We observed that MKN and FOMM also provided good results, especially on MSE metric, e.g., 37.1098 and 37.3648 in Table VIII.

C. Ablation Study

To better understand the merits of designs of DFC-Net, we conducted detailed ablation studies on *Subject1* from EDN-10K and *Liam* from MIXAMO-POSE. The evaluation results are shown in Tables IX and X.

Method	<i>Andromeda</i>	<i>Liam</i>	<i>Remy</i>	<i>Stefani</i>	Average
NN	24.9047	28.4846	27.1801	24.8609	26.3576
CycleGAN	27.5520	29.9436	28.2237	22.7682	27.1219
Pix2Pix	23.9370	23.5610	24.0687	21.5841	23.2877
EDN	24.3244	23.1203	23.9229	35.0930	26.6151
LWG	24.2905	22.8587	22.9707	22.0910	23.0527
MKN	30.5934	39.3444	29.4817	24.1297	30.8873
FOMM	27.7809	29.0469	27.4474	25.3934	28.6544
Ours	23.8539	21.7328	22.0763	21.2587	22.2304

TABLE I: Comparisons on MIXAMO-POSE in terms of MSE with the best results (lowest values) in bold.

Method	<i>Andromeda</i>	<i>Liam</i>	<i>Remy</i>	<i>Stefani</i>	Average
NN	0.7357	0.7265	0.7487	0.7411	0.7380
CycleGAN	0.7205	0.7154	0.7377	0.7753	0.7372
Pix2Pix	0.7784	0.7955	0.7932	0.8069	0.7935
EDN	0.7817	0.7931	0.7926	0.8058	0.7933
LWG	0.7613	0.7912	0.7887	0.7858	0.7817
MKN	0.7076	0.6874	0.7531	0.7753	0.7308
FOMM	0.7165	0.7404	0.7538	0.7464	0.7392
Ours	0.7726	0.8040	0.8057	0.8071	0.7973

TABLE II: Comparisons on MIXAMO-POSE in terms of SSIM with best results (highest values) in bold.

Method	<i>Andromeda</i>	<i>Liam</i>	<i>Remy</i>	<i>Stefani</i>	Average
NN	34.4420	34.0575	34.3865	34.3977	34.3209
CycleGAN	33.7903	33.4230	33.6786	34.6130	33.8762
Pix2Pix	34.4049	34.5167	34.3875	34.8497	34.5397
EDN	34.3524	34.5882	34.4214	34.7247	34.5217
LWG	34.3426	34.6762	34.6183	34.7519	34.5972
MKN	33.6626	32.8841	33.7487	34.4779	33.6933
FOMM	33.7777	33.5912	33.8337	34.1919	33.8486
Ours	34.4336	34.8798	34.7823	34.9303	34.7565

TABLE III: Comparisons on MIXAMO-POSE in terms of PSNR with the best results (highest values) in bold.

Method	MSE(↓)	PSNR(↑)	SSIM(↑)
NN	26.3576	34.3209	0.7380
CycleGAN	27.1219	33.8762	0.7372
Pix2Pix	23.2877	34.5397	0.7935
EDN	26.6151	34.5217	0.7933
LWG	23.0527	34.5972	0.7817
MKN	30.8873	33.6933	0.7308
FOMM	28.6544	33.8486	0.7392
Ours	22.2304	34.7565	0.7973

TABLE IV: Comparisons of average results on MIXAMO-POSE with best results in bold.

1) *Keypoint Amplifier*: The results in the second row versus those in the first row showed that the keypoint amplifier strengthened the performance of pose transfer. Even with the consistency losses and support set (rows 6 and 7), it continuously reduced the interference of the noise on the keypoint heatmaps.

2) *Consistency Losses*: We explored the effects of consistency losses on the task of pose transfer. Considering the different results between the second row and the third row, the static feature consistency loss \mathcal{L}_{sc} boosted the pose trans-

Method	<i>Subject1</i>	<i>Subject2</i>	<i>Subject3</i>	<i>Subject4</i>	Average
NN	54.9448	36.2267	55.2041	26.2531	43.1572
CycleGAN	64.1959	77.4336	70.3681	52.5171	66.1287
Pix2Pix	58.3633	43.0771	62.0203	24.1688	46.9074
EDN	56.3549	36.3887	55.9625	21.5724	42.5696
LWG	51.6246	43.2884	53.4031	21.4314	42.4368
MKN	48.1603	30.9902	47.6255	21.6634	37.1098
FOMM	46.2852	30.7603	51.1431	21.2709	37.3648
Ours	45.2043	30.4782	48.5436	20.7248	36.2377

TABLE V: Comparisons on EDN-10k in terms of MSE with the best results (lowest values) in bold.

Method	<i>Subject1</i>	<i>Subject2</i>	<i>Subject3</i>	<i>Subject4</i>	Average
NN	0.6138	0.8253	0.7616	0.8437	0.7611
CycleGAN	0.5256	0.4911	0.5869	0.7821	0.5964
Pix2Pix	0.6238	0.8040	0.7585	0.8767	0.7658
EDN	0.6205	0.8445	0.8233	0.8939	0.7956
LWG	0.6394	0.8375	0.7434	0.8634	0.7709
MKN	0.7007	0.8503	0.8030	0.8904	0.8111
FOMM	0.6645	0.8445	0.7896	0.8649	0.7908
Ours	0.7083	0.8670	0.8241	0.9083	0.8269

TABLE VI: Comparisons on EDN-10k in terms of SSIM with the best results (highest values) in bold.

Method	<i>Subject1</i>	<i>Subject2</i>	<i>Subject3</i>	<i>Subject4</i>	Average
NN	30.7957	32.6439	31.3307	34.2481	32.2546
CycleGAN	30.0577	29.2421	29.7007	31.3398	30.0851
Pix2Pix	30.6020	32.0304	30.5843	34.6860	31.9757
EDN	30.7109	32.8639	30.9957	35.0369	32.4019
LWG	31.0085	31.7812	31.0503	35.0118	32.2129
MKN	31.3094	33.2530	30.6493	34.9108	32.5306
FOMM	31.5272	33.3145	31.3099	34.9612	32.7782
Ours	31.5978	33.3509	31.4159	35.0718	32.8591

TABLE VII: Comparisons on EDN-10k in terms of PSNR with the best results (highest values) in bold.

Method	MSE(\downarrow)	PSNR(\uparrow)	SSIM(\uparrow)
NN	43.1572	32.2546	0.7611
CycleGAN	66.1287	30.0851	0.5964
Pix2Pix	46.9074	31.9757	0.7658
EDN	42.5696	32.4019	0.7956
LWG	42.4368	32.2129	0.7709
MKN	37.1098	32.5306	0.8111
FOMM	37.3648	32.7782	0.7908
Ours	36.2377	32.8591	0.8269

TABLE VIII: Comparisons of average results on EDN-10k with best results in bold.

fer task and verified its validity. Moreover, the performance variations between the second row and the fourth row clearly evidenced the advantages of pose feature consistency loss \mathcal{L}_{mc} .

3) *Support Set*: Finally, we added the support set and utilized the loss \mathcal{L}_{sup} during the training. The comparisons among the final row and other rows notably indicated that the support set could improve the generalization ability and the robustness of our model, especially when the poses of the source person are closer to the poses in the support set. The support set provided more negative examples besides

	KA	\mathcal{L}_{sc}	\mathcal{L}_{mc}	\mathcal{L}_{sup}	MSE(\downarrow)	PSNR(\uparrow)	SSIM(\uparrow)
1					52.5749	30.9361	0.6595
2	✓				50.7810	31.0860	0.6676
3	✓	✓			49.3831	31.2043	0.6742
4	✓		✓		49.8352	31.1662	0.6710
5	✓	✓	✓		48.6431	31.2714	0.6796
6		✓	✓	✓	46.3699	31.4801	0.6937
7	✓	✓	✓	✓	45.2043	31.5978	0.7083

TABLE IX: Ablation studies on *Subject1* from EDN-10k. KA denotes the Keypoint Amplifier.

	KA	\mathcal{L}_{sc}	\mathcal{L}_{mc}	\mathcal{L}_{sup}	MSE(\downarrow)	PSNR(\uparrow)	SSIM(\uparrow)
1					26.4595	33.9856	0.7605
2	✓				24.7312	34.2838	0.7726
3	✓	✓			23.7580	34.4666	0.7830
4	✓		✓		22.6160	34.6913	0.8011
5	✓	✓	✓		21.9509	34.8292	0.8032
6		✓	✓	✓	22.0240	34.8047	0.8031
7	✓	✓	✓	✓	21.7328	34.8798	0.8040

TABLE X: Ablation studies on *Liam* from MIXAMO-POSE. KA denotes the Keypoint Amplifier.

the original training set and could help the discriminator to form an accurate boundary, which could further strengthen the performance of the generator.

D. Qualitative Results

We further highlighted the superiority of our proposed approach by showing and contrasting the visualizations of synthesized results of all models on MIXAMO-POSE and EDN-10k, respectively. In addition, we presented the visualizations of the ablation comparisons for *Subject1* on EDN-10k to indicate the effectiveness of components of DFC-Net.

1) *Visual comparisons on MIXAMO-POSE*: As depicted in Figure 2, we employed multiple target persons and source persons with various poses that were different from those in the training set of the MIXAMO-POSE. Compared with the aforementioned baselines, DFC-Net offered better transfer results and alleviated their drawbacks on synthesizing body parts, clothes, faces, just name a few. We illustrate details as follows:

- Firstly, only DFC-Net generated the left hand of *Liam* at the 1st and 2nd rows while there were only the arm in results of other baselines.
- Meanwhile, images produced by EDN had stale colors and lots of noisy pixels in terms of clothes and faces, and it failed to capture the details of shoes at the 3rd row since the color of shoes is white and is easily confused with the background.
- Moreover, even the image results of NN are more clear and not blurry, the NN method always made incorrect pose transfer since it can solely synthesize poses existed in the training set.
- The CycleGAN could provide similar poses compared with the ground-truths, the poses were distorted and the qualities of corresponding images were constantly degraded.

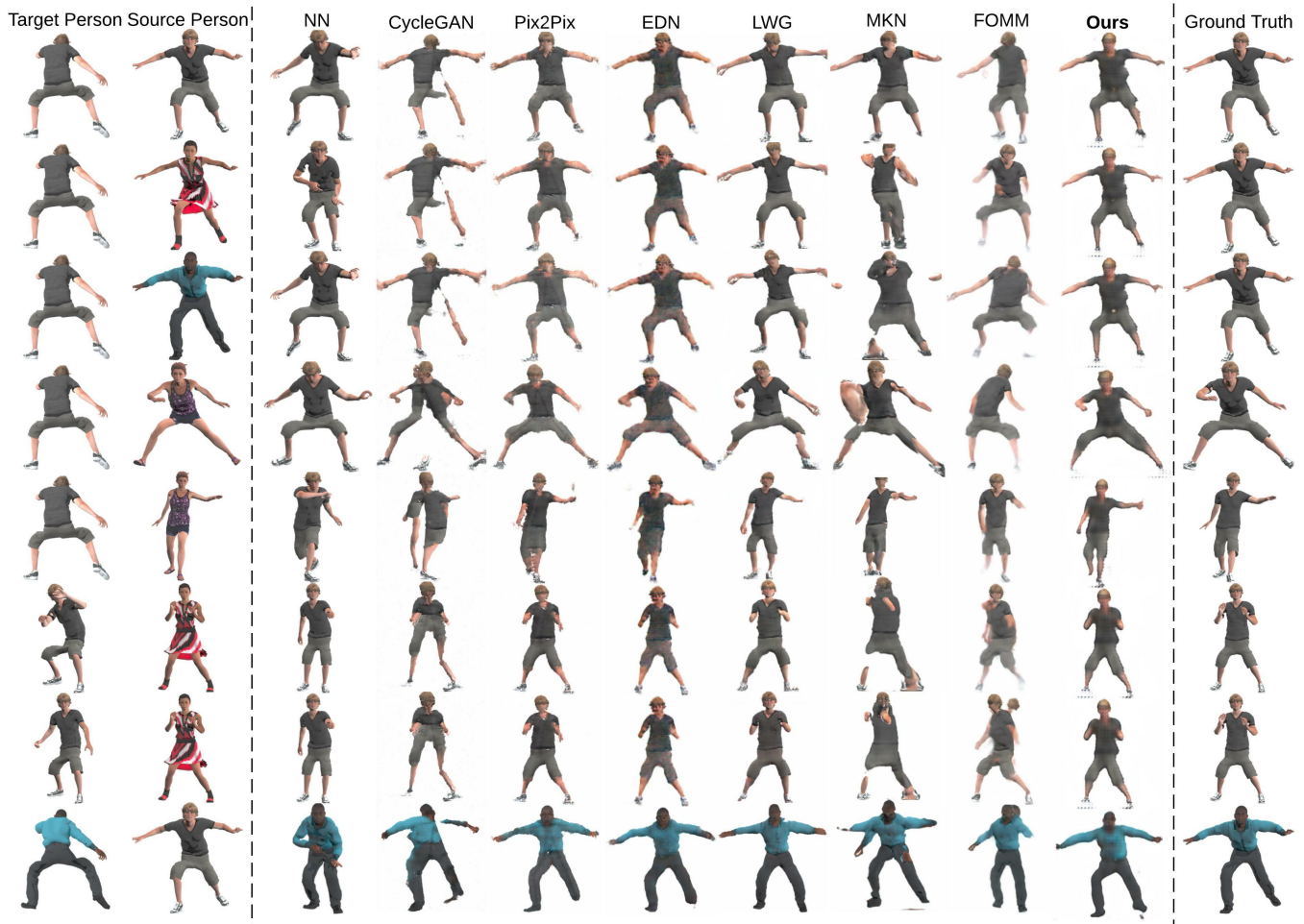


Fig. 2: Visualizations of motion transfer with different characters and various motions on MIXAMO-POSE. The columns from left to right show target persons, source persons, results of different methods, and ground truth, respectively.

- Besides, though the Pix2Pix and EDN could synthesize the target persons with the desired poses, some body parts (e.g., arms, hands) generated by Pix2Pix were severely corrupted.

2) *Visual comparisons on EDN-10K*: We also provided visualization results on EDN-10K in Figure 3 and cropped the results in Figure 4 with more details, and DFC-Net synthesized real person image results with better qualities, which clearly indicated the effectiveness of our method as well. For instance:

- The results produced by Pix2Pix and EDN were more blurry and there was an aliasing effect on the edges of the subject in the Pix2Pix result.
- Sometimes NN could generate images that are closer to the ground-truths, e.g. image of *Subject3* at the third row of Figure 3, since the number of images in the training set increases from 1488 to 10000. But people could still easily determine that the poses of the generated images are different from the ground-truths.
- In addition, EDN showed better image results than Pix2Pix did. In the third row of Figure 3, we noticed that the image of *Subject3*, synthesized by Pix2Pix, had much noise in the subject’s hair. On the contrary, the result of EDN was smoother and more realistic, but they

lacked many details compared with DFC-Net, especially the face part was still twisted.

- As depicted in Figure 4, we observed that the synthesized images of our method contained more details, including the clear face, wrinkles on clothes, etc.

3) *Visual ablation studies on Subject1*: We presented the visualization of the ablation study results on *Subject1* in Figure 5. In which we observed that each component has different degrees of improvement to the results, including clear head, hand gesture, etc. Specifically:

- As shown in the column of setting 7, DFC-Net with full components synthesized images with more accurate details and better qualities.
- The results produced by setting 1, which does not have the Keypoint Amplifier, have much noise than other settings, especially near the head area.

V. CONCLUSION

In this paper, we proposed DFC-Net, a novel network with disentangled feature consistencies for human pose transfer. We introduce two disentangled feature consistency losses to enforce the pose and static information to be consistent between the synthesized and real images. Besides, we leverage the



Fig. 3: Visualizations of pose transfer with different characters and various poses on EDN-10K. The columns from left to right show target persons, source persons, results of different methods, and ground truth, respectively.

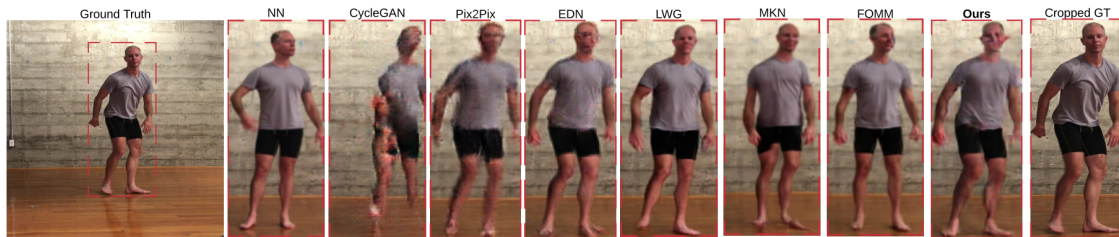


Fig. 4: Visualizations of *Subject1* from EDN-10K with more details. We cropped the results to the areas surrounded by the red dash lines.

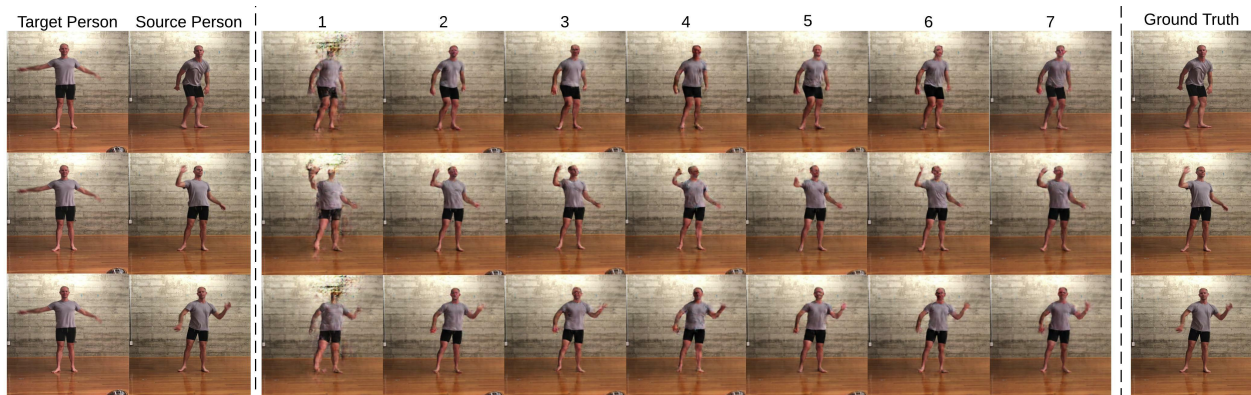


Fig. 5: Visualizations of *Subject1* from EDN-10K. The columns from left to right show target persons, source persons, results of 6 different settings in ablation studies, and ground truth, respectively. The indices of each column are the same as in the Table X.

keypoint amplifier to denoise the keypoint heatmaps and make it easier to extract the pose features. Moreover, we show that the support set MIXAMO-SUP containing different subjects with unseen poses can boost the pose transfer performance and enhance the robustness of the model. To enable the accurate evaluation of pose transfer between different people, we collect an animation character dataset MIXAMO-POSE. Results on both animation and real image datasets, MIXAMO-POSE and EDN-10K, consistently demonstrated the effectiveness of the proposed model.

REFERENCES

- [1] H.-Y. Tung, H.-W. Tung, E. Yumer, and K. Fragkiadaki, “Self-supervised learning of motion capture,” in *Advances in Neural Information Processing Systems*, 2017, pp. 5236–5246.
- [2] L. Liu, W. Xu, M. Zollhoefer, H. Kim, F. Bernard, M. Habermann, W. Wang, and C. Theobalt, “Neural rendering and reenactment of human actor videos,” *ACM Transactions on Graphics*, 2019.
- [3] S. Xia, L. Gao, Y.-K. Lai, M.-Z. Yuan, and J. Chai, “A survey on human performance capture and animation,” *Journal of Computer Science and Technology*, 2017.
- [4] T. B. Moeslund, A. Hilton, and V. Krüger, “A survey of advances in vision-based human motion capture and analysis,” *Computer vision and image understanding*, 2006.

- [5] I. Goodfellow, J. Pouget-Abadie, M. Mirza, B. Xu, D. Warde-Farley, S. Ozair, A. Courville, and Y. Bengio, "Generative adversarial nets," in *NIPS*, 2014.
- [6] Y. Liu, Q. Sun, X. He, A.-A. Liu, Y. Su, and T.-S. Chua, "Generating face images with attributes for free," *IEEE Transactions on Neural Networks and Learning Systems*, 2020.
- [7] S. Jiang, J. Li, and Y. Fu, "Deep learning for fashion style generation," *IEEE Transactions on Neural Networks and Learning Systems*, 2021.
- [8] P. Isola, J.-Y. Zhu, T. Zhou, and A. A. Efros, "Image-to-image translation with conditional adversarial networks," in *CVPR*, 2017.
- [9] J.-Y. Zhu, T. Park, P. Isola, and A. A. Efros, "Unpaired image-to-image translation using cycle-consistent adversarial networks," in *ICCV*, 2017.
- [10] A. Newell, K. Yang, and J. Deng, "Stacked hourglass networks for human pose estimation," in *ECCV*, 2016.
- [11] S.-E. Wei, V. Ramakrishna, T. Kanade, and Y. Sheikh, "Convolutional pose machines," in *CVPR*, 2016.
- [12] Z. Cao, T. Simon, S.-E. Wei, and Y. Sheikh, "Realtime multi-person 2d pose estimation using part affinity fields," in *CVPR*, 2017.
- [13] Z. Cao, G. Hidalgo Martinez, T. Simon, S. Wei, and Y. A. Sheikh, "Openpose: Realtime multi-person 2d pose estimation using part affinity fields," *IEEE Transactions on Pattern Analysis and Machine Intelligence*, 2019.
- [14] K. Aberman, R. Wu, D. Lischinski, B. Chen, and D. Cohen-Or, "Learning character-agnostic motion for motion retargeting in 2d," *ACM Transactions on Graphics (TOG)*, 2019.
- [15] Adobe Systems Inc., <https://www.mixamo.com>, 2018, accessed: 2018-12-27.
- [16] C. Chan, S. Ginosar, T. Zhou, and A. A. Efros, "Everybody dance now," in *ICCV*, 2019.
- [17] M. Mirza and S. Osindero, "Conditional generative adversarial nets," *arXiv preprint arXiv:1411.1784*, 2014.
- [18] G. E. Hinton and R. R. Salakhutdinov, "Reducing the dimensionality of data with neural networks," *science*, 2006.
- [19] Z. Yi, H. Zhang, P. Tan, and M. Gong, "Dualgan: Unsupervised dual learning for image-to-image translation," in *ICCV*, 2017.
- [20] Y. Hoshen and L. Wolf, "Identifying analogies across domains," in *ICLR*, 2018.
- [21] M.-Y. Liu, T. Breuel, and J. Kautz, "Unsupervised image-to-image translation networks," in *NIPS*, 2017.
- [22] K. Bousmalis, N. Silberman, D. Dohan, D. Erhan, and D. Krishnan, "Unsupervised pixel-level domain adaptation with generative adversarial networks," in *CVPR*, 2017.
- [23] X. Huang, M.-Y. Liu, S. Belongie, and J. Kautz, "Multimodal unsupervised image-to-image translation," in *ECCV*, 2018.
- [24] C. Lassner, G. Pons-Moll, and P. V. Gehler, "A generative model of people in clothing," in *Proceedings of the IEEE International Conference on Computer Vision*, 2017.
- [25] Z. Zhu, T. Huang, B. Shi, M. Yu, B. Wang, and X. Bai, "Progressive pose attention transfer for person image generation," in *CVPR*, 2019.
- [26] Y. Li, C. Huang, and C. C. Loy, "Dense intrinsic appearance flow for human pose transfer," in *CVPR*, 2019.
- [27] L. Ma, X. Jia, Q. Sun, B. Schiele, T. Tuytelaars, and L. Van Gool, "Pose guided person image generation," in *NIPS*, 2017.
- [28] L. Ma, Q. Sun, S. Georgoulis, L. Van Gool, B. Schiele, and M. Fritz, "Disentangled person image generation," in *CVPR*, 2018.
- [29] G. Balakrishnan, A. Zhao, A. V. Dalca, F. Durand, and J. Guttag, "Synthesizing images of humans in unseen poses," in *CVPR*, 2018.
- [30] M. Jaderberg, K. Simonyan, A. Zisserman *et al.*, "Spatial transformer networks," in *NIPS*, 2015.
- [31] C. Si, W. Wang, L. Wang, and T. Tan, "Multistage adversarial losses for pose-based human image synthesis," in *CVPR*, 2018.
- [32] N. Neverova, R. Alp Guler, and I. Kokkinos, "Dense pose transfer," in *ECCV*, 2018.
- [33] R. Alp Güler, N. Neverova, and I. Kokkinos, "Densepose: Dense human pose estimation in the wild," in *CVPR*, 2018.
- [34] T.-C. Wang, M.-Y. Liu, J.-Y. Zhu, A. Tao, J. Kautz, and B. Catanzaro, "High-resolution image synthesis and semantic manipulation with conditional gans," in *CVPR*, 2018.
- [35] A. Siarohin, E. Sangineto, S. Lathuilière, and N. Sebe, "Deformable gans for pose-based human image generation," in *CVPR*, 2018.
- [36] A. Siarohin, S. Lathuilière, S. Tulyakov, E. Ricci, and N. Sebe, "Animating arbitrary objects via deep motion transfer," in *CVPR*, 2019.
- [37] A. Siarohin, S. Lathuilière, S. Tulyakov, E. Ricci, and N. Sebe, "First order motion model for image animation," in *NIPS*, 2019.
- [38] W. Liu, Z. Piao, J. Min, W. Luo, L. Ma, and S. Gao, "Liquid warping gan: A unified framework for human motion imitation, appearance transfer and novel view synthesis," in *ICCV*, 2019.
- [39] M. Loper, N. Mahmood, J. Romero, G. Pons-Moll, and M. J. Black, "Smpl: A skinned multi-person linear model," *ACM transactions on graphics (TOG)*, 2015.
- [40] T.-Y. Lin, M. Maire, S. Belongie, J. Hays, P. Perona, D. Ramanan, P. Dollár, and C. L. Zitnick, "Microsoft coco: Common objects in context," in *ECCV*, 2014.
- [41] J. Johnson, A. Alahi, and L. Fei-Fei, "Perceptual losses for real-time style transfer and super-resolution," in *ECCV*, 2016.
- [42] K. Simonyan and A. Zisserman, "Very deep convolutional networks for large-scale image recognition," *arXiv preprint arXiv:1409.1556*, 2014.
- [43] —, "Very deep convolutional networks for large-scale image recognition," *arXiv preprint arXiv:1409.1556*, 2014.
- [44] T.-C. Wang, M.-Y. Liu, J.-Y. Zhu, G. Liu, A. Tao, J. Kautz, and B. Catanzaro, "Video-to-video synthesis," in *NIPS*, 2018.
- [45] K. He, X. Zhang, S. Ren, and J. Sun, "Deep residual learning for image recognition," in *CVPR*, 2016.
- [46] Blender Online Community, *Blender - a 3D modelling and rendering package*, Blender Foundation, Stichting Blender Foundation, Amsterdam, 2018. [Online]. Available: <http://www.blender.org>
- [47] G. Bradski, "The OpenCV Library," *Dr. Dobb's Journal of Software Tools*, 2000.
- [48] Z. Wang, A. C. Bovik, H. R. Sheikh, E. P. Simoncelli *et al.*, "Image quality assessment: from error visibility to structural similarity," *IEEE transactions on image processing*, 2004.



Kun Wu received his B.S. degree from Beijing Institute of Technology in 2017. He is currently working towards his Ph.D degree in the Department of Electrical Engineering and Computer Science at Syracuse University. His research interests include Machine Learning and Computer Vision.



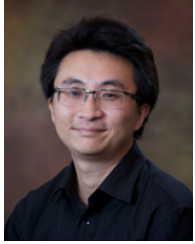
Chengxiang Yin received his B.S. degree from Beijing Institute of Technology in 2016. He is currently working toward his Ph.D degree in the Department of Electrical Engineering and Computer Science at Syracuse University. His research interests include Machine Learning and Computer Vision.



Zhengping Che received the Ph.D. degree in Computer Science from the University of Southern California, Los Angeles, CA, USA, in 2018, and the B.Eng. degree in Computer Science from Tsinghua University, Beijing, China, in 2013. He is a research scientist at Didi Chuxing. His current research interests lie in the areas of machine learning and deep learning with applications to autonomous driving, intelligent transportation, cognitive intelligence, and efficient learning.



Bo Jiang received the master degree from the Department of Computer Science, University of Southern California, USA, in 2017. He is a research scientist at Didi Chuxing. His research interests include machine learning and deep learning.



Jian Tang received his Ph.D degree in Computer Science from Arizona State University in 2006. He is an IEEE Fellow and an ACM Distinguished Member. He is with Midea Group. His research interests lie in the areas of AI, IoT, Wireless Networking, Mobile Computing and Big Data Systems. Dr. Tang has published over 160 papers in premier journals and conferences. He received an NSF CAREER award in 2009. He also received several best paper awards, including the 2019 William R. Bennett Prize and the 2019 TCBD (Technical Committee on

Big Data) Best Journal Paper Award from IEEE Communications Society (ComSoc), the 2016 Best Vehicular Electronics Paper Award from IEEE Vehicular Technology Society (VTS), and Best Paper Awards from the 2014 IEEE International Conference on Communications (ICC) and the 2015 IEEE Global Communications Conference (Globecom) respectively. He has served as an editor for several IEEE journals, including IEEE Transactions on Big Data, IEEE Transactions on Mobile Computing, etc. In addition, he served as a TPC co-chair for a few international conferences, including the IEEE/ACM IWQoS'2019, MobiQuitous'2018, IEEE iThings'2015. etc.; as the TPC vice chair for the INFOCOM'2019; and as an area TPC chair for INFOCOM 2017-2018. He is also an IEEE VTS Distinguished Lecturer, and the Chair of the Communications Switching and Routing Committee of IEEE ComSoc.



Zheng Guan is an assistant teacher of Beijing Institute of Technology, graduated from Beijing Institute of Technology Computer Science School. His interest areas are simulation systems, embedded systems, and artificial intelligence.



Gangyi Ding is a professor of Beijing Institute of Technology. His interest areas are simulation systems, embedded systems, and artificial intelligence.